Journal of Materials Chemistry A

Accepted Manuscript

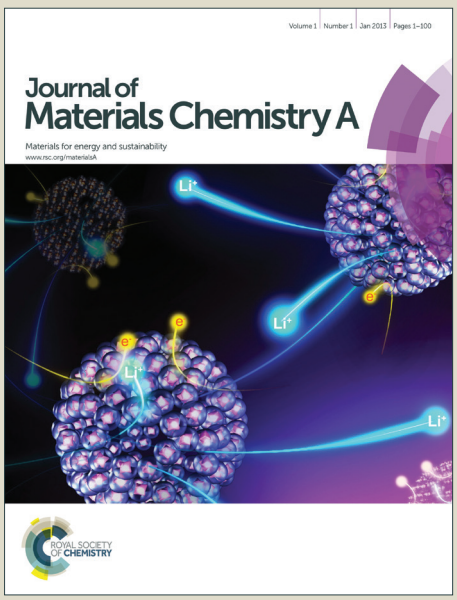

ROYAL SOCIETY OF CHEMISTRY

www.rsc.org/materialsA

DES Assisted Synthesis of Hierarchical Nitrogen-Doped Carbon Molecular Sieves for Selective CO_2 versus N_2 Adsorption

J. Patiño,[a] M. C. Gutiérrez,[a] D. Carriazo,[a] C. O. Ania,[b] J. L. G. Fierro,[c] M. L. Ferrer,[a] and F. del Monte [a,*]

[a] Instituto de Ciencia de Materiales de Madrid-ICMM
Consejo Superior de Investigaciones Científicas-CSIC.
Campus de Cantoblanco
28049-Madrid (Spain)
E-mail: delmonte@icmm.csic.es

[b] Instituto Nacional del Carbon-INCAR
Consejo Superior de Investigaciones Científicas-CSIC.
C/Francisco Pintado Fe, 26.
33011-Oviedo (Spain)

[c] Instituto de Catálisis y Petroleoquímica-ICP
Consejo Superior de Investigaciones Científicas-CSIC.
Campus de Cantoblanco
28049-Madrid (Spain)

Abstract

Deep eutectic solvents (DESs) composed of resorcinol, 3-hydroxypyridine and tetraethylammonium bromide were used for the synthesis of hierarchical nitrogen-doped carbon molecular sieves. DESs played a multiple role in the synthetic process: the liquid medium that ensured reagents homogenization, the structure-directing agent responsible for the achievement of the hierarchical structure, and the source of carbon and nitrogen of the solid sorbent obtained after carbonization. Thus, the synthesis offers an economy of reagents that emphasized the green aspects and low cost of conventional polycondensations. Interestingly, while macropores facilitated mass transport and accessibility to the surface area, the combination of molecular-sieve-structure and nitrogen functionalization provided, respectively, excellent CO_2-adsorption capacities – of up to 3.7 mmol/g – and outstanding CO_2-N_2 selectivities – of up to 14.4 from single component gas data. Nonetheless, the CO_2-N_2 selectivity in the Henry law regime – representative of post-combustion flue-gas streams – of some of our carbons was particularly remarkable (e.g. 96), in range to or even higher than those described for most recent carbons and only surpassed by certain zeolites.

Introduction

Mitigation of global climate change needs of an urgent and drastic reduction of carbon dioxide emission from combustion of fossil fuels. Among other technologies,[1] number of solid sorbents including zeolites,[2, 3] functionalized porous silica,[4] metal–organic frameworks (MOFs),[5, 6, 7] and carbonaceous materials[8, 9] have proved effective for carbon capture and storage (CCS). There is not an ideal adsorbent, and each one shows its particular advantages and drawbacks. Nonetheless, our opinion is that the use of carbon-based materials is especially promising because of their relatively low cost and easy regeneration. For instance, carbons obtained by direct carbonization of either petroleum pitch[10] or biomass[11, 12, 13] have exhibited CO_2-adsorption capabilities close to the best ones ever reported for non-carbonaceous adsorbents. The yet advantage of the latter ones resides in their synthetic origin so that one can prepare them with tailor-made high surface areas and surface functionalities. It is worth noting that these features provide not only high CO_2-adsorption capability but also extraordinary selectivity for gas separation purposes.

Within this context, synthetic carbons are particularly interesting because of the possibility to enhance their original performance in terms of both CO_2-adsorption capability and selectivity by introducing nitrogen functionalities – to which CO_2 exhibits a particular adsorption affinity – and/or creating narrow micropores – through which CO_2 diffusion is not restricted.[14] In structural terms, hierarchical porous carbons (HPCs) are also attracting much attention because of the combination of high surface area and pore volume – provided by micro- and small mesopores – and accessibility to these active sites – provided by macro- and medium/large mesopores.[15] Unfortunately, conventional polycondensations typically need of the use of certain additives (e.g. block-copolymers) as structure directing agents[16, 17] raising concerns about the low cost of the resulting materials. Block-copolymer recovering (e.g. washing out) after polycondensation and reuse could be an option but this is by no means trivial because of the impeded diffusion of pseudo-high molecular weight substances through small pores. Actually, recent reports demonstrate that the design of sustainable synthetic routes that allow the preparation of carbonaceous adsorbents with tailor-made hierarchical structures and surface functionalities is yet challenging.[18]

The formation of eutectic mixtures (described as either deep eutectic solvents – DESs – by Abbott and coworkers,[19, 20, 21, 22] or low-transition-temperature mixtures – LTTMs – by Kroon and coworkers)[23] using some of the most typical synthetic precursors for carbon preparation has also opened interesting perspectives in this field. For instance, the use of DESs based on mixtures of resorcinol (Re) and choline chloride (ChCl) allowed, upon polycondensation with formaldehyde and without the use of further additives, the formation of monolithic carbons built of highly cross-linked clusters that aggregated and assembled into a stiff and interconnected hierarchical structure.[24] In this case, the bicontinuous porous structure was obtained via a spinodal decomposition process where one of the components forming the DES (e.g. Re) acted as precursor of the polymer phase while the second one (e.g. ChCl) was segregated into the polymer depleted phase. The high conversion in which resorcinol becomes the material itself and the feasible recovery of ChCl – and hence, its reuse in subsequent reactions – make DES-assisted syntheses very efficient in terms of reagent economy.[25] Interestingly, the wide range of DES that can be prepared from not only resorcinol but also other synthetic precursors provides a remarkable versatility – in both structural and compositional terms – to the carbons that can be obtained through this synthetic approach.[26, 27, 28, 29] For instance, and with regard to the preparation of carbons for CO_2 adsorption, we have recently reported how hierarchical nitrogen-doped carbons (HNCs) can be obtained upon the use of DES containing resorcinol and 3-hydroxypyridine (Hy)[30] while DES containing resorcinol and 4-hexylresorcinol can form hierarchical carbon molecular sieves (HCMSs).[31] Both materials were suitable as CO_2 adsorbents, with sorption capability and selectivity in range to those reported for other sorbents.

Herein, we further explored the versatility of DES-assisted syntheses for preparation of hierarchical nitrogen-doped carbon molecular sieves (HNCMSs). The DESs of choice were composed of Re, Hy and tetraethylammonium bromide (TEA) with 1:2:1 and 1:3:1.75 molar ratios. DESs formation was studied by ^{1}H NMR spectroscopy and differential scanning calorimetry (DSC). Compared to our previous work on HNCs, the Hy to Re molar ratio at DES was increased from 1:1[30] to either 1:2 or 1:3. This approach, in combination with the investigation of different carbonization temperatures (e.g. 450, 500, 600, 700, and 800°C)[32, 33] allowed enhancing the nitrogen

content of the resulting carbons and hence, their CO_2-sorption capabilities. Furthermore, we herein report on the use of TEA-based DESs for the formation of carbons with a molecular-sieve-like microporous network, inspired by its common use as structure directing agents in zeolites[34, 35] and HCMS preparation.[31] Formaldehyde addition promoted Re and Hy polycondensation, the extension of which was assessed by ^{13}C NMR and FTIR spectroscopies. The macroporous structure of the carbons resulting after thermal treatment in nitrogen atmosphere was studied by scanning electron microscopy (SEM) while the microporous textural properties were evaluated by gas adsorption (N_2 at 77K and CO_2 at 273K). The CO_2 adsorption capability of the resulting carbons was investigated from equilibrium adsorption isotherms at 25°C, evaluating the CO_2/N_2 selectivity at the equilibrium, using Henry constants and the Ideal Adsorbed Solution Theory (IAST) equation.

Experimental Part

Preparation of deep eutectic solvents (DESs)

DESs (e.g. DES-ReHy12 and DES-ReHy13) were obtained upon thermal treatment (at 90°C overnight) of the physical mixture of the individual components, resorcinol (Re, T_m = 110°C), 3-hydroxypyridine (Hy, T_m = 129°C) and tetraethylammonium bromide (TEA, T_m = 286°C) in 1:2:1 and 1:3:1.75 molar ratios, respectively.

Preparation of carbons

DES-ReHy12 and DES-ReHy13 were mixed with an aqueous solution of formaldehyde (37 wt%) for a F/(Re + Hy) molar ratio of 2.0. Polycondensations were catalysed by addition of 15.7 μL Na_2CO_3 dissolved in water (140 mg/mL) per mmol of carbon precursor (e.g. Re+Hy). The DES content in the aqueous dilution obtained after catalyst addition was 59.5 and 62.2 wt% for DES-ReHy12 and DES-ReHy13, respectively. After stirring for 5 min, the resulting mixtures were aged for two hours at room temperature and, afterwards, thermally treated (first 6 h at 60°C and then, 7 days at 90°C) in closed containers to prevent solvent evaporation. The resulting gels were washed three times in water (35 mL) for TEA recovery. The washed gels were thermally treated under N_2 atmosphere to 210°C for 4 h and then either to 450, 500,

600, 700, or 800°C for another 4 hours (the heating ramp was 1.0°C/min). The resulting carbons were named as C_{ReHynm}@Z where n and m stand respectively for the relative molar equivalents of Re and Hy, and Z for the temperature used for carbonization.

Samples characterization

DSC traces were obtained using a TA Instruments Model DSC Q-100 system. The samples were run under nitrogen atmosphere on an aluminium pan in a sealed furnace, stabilized for 5 min at 20°C, and then cooled to -90°C before heating at a rate of 5°C/min. ^{1}H NMR spectra were recorded on a Bruker spectrometer DRX-500. DESs were placed in capillary tubes, using deuterated chloroform ($CDCl_3$) as an external reference (the deuterium signal was used for locking and shimming the sample). FTIR spectra were recorded on a BrukerModel IFS60v. Solid- state ^{13}C-CPMAS-NMR spectra were recorded on a BrukerAV-400-WB spectrometer, using a standard cross-polarization pulse sequence. The morphology of the resulting carbons was studied by scanning electron microscopy (SEM) using a SEM Zeiss DSM-950 instrument.

The nanotexture of the prepared carbons was characterized by measuring the N_2 (ASAP 2020, Micromeritics) and CO_2 (Tristar 3200, Micromeritics) adsorption–desorption isotherms at 77 and 273 K, respectively. The samples were previously outgassed under dynamic vacuum (ca. 10^{-5} Torr) at 373 K for 6 hours. The isotherms were used to evaluate the specific surface area (BET equation). The volume of narrow micropores was evaluated from the DR formulism applied to the CO_2 adsorption data at 273 K, using 1.023 g/cm^3 as the density of adsorbed CO_2 and 0.36 as the value of the β parameter.

Adsorption–desorption isotherm measurements of N_2 and CO_2 were also performed at ambient temperature (298 K) in the pressure range of 0.1–900 Torr using the above-mentioned outgassing conditions. The analyser was equipped with a pressure transducer of capacity 1000 mmHg (accuracy within 0.15% of reading). Strict analysis conditions were programmed during the gas adsorption measurements to assure equilibrium data in all gases, while each isotherm measurement was performed in duplicate to guarantee the accuracy of the experiments (error was below 0.1%) and to obtain reproducible data. During the analysis, the adsorption temperature was maintained using a circulating-oil bath at a constant temperature. Air Products

supplied all gases with an ultrahigh purity (i.e., 99.9992%). The Henry's constants were obtained by fitting the adsorption data to a Virial-type expression: [36]

$$\ln(P/V) = A_0 + A_1V + A_2V$$

where P is the pressure, V is the adsorbed amount, T is the temperature, and Ai are the Virial coefficients required to adequately describe the isotherms. From these results, the Henry's constant (k_H) can be calculated as:

$$k_H = \exp(-A_0).$$

The Henry's law selectivity for gas component i over j at a given temperature was calculated using the equation $S_{ij} = K_{Hi}/K_{Hj}$. The selectivity, as the ratio between the single gas uptake obtained from the equilibrium adsorption data, was measured at 25°C and 1 atm and under equilibrium conditions.

IAST was used to predict binary mixture adsorption from the experimental pure-gas isotherms.[37] The integration required by IAST was achieved by fitting the single-component gas isotherms to the Jensen equation.[38] Typical conditions of flue gases in post-combustion processes (e.g. CO_2–N_2 mixtures of 15/85) as well as equimolecular mixtures (e.g. 50/50) were used in the binary mixture predictions. Equimolecular mixtures (e.g. 50/50) of CO_2–N_2 were also analysed.

X-Ray Photoelectron (XPS) spectroscopy surface analysis was performed in a VG ESCALAB 200R electron spectrometer equipped with a hemispherical electron analyser and an Al Kα ($h\upsilon$ = 1486.6 eV, 1 eV = $1.6302\cdot10^{-19}$ J) 120 watts X-ray source. Samples were carbon glued on 8 mm diameter stainless steel troughs mounted on a sample rod placed in the pre-treatment chamber and degassed for 0.5 h prior to being transferred to the analysis chamber. The base pressure in the analysis chamber was maintained below 4×10^{-9} mbar during data acquisition. The pass energy of the analyser was set at 50 eV. The binding energies were referenced to the binding energy of C1s core-level spectrum at 284.9 eV. Data processing was performed with the XPS peak program, the spectra were decomposed with the least squares fitting routine provided with the

software with Gaussian/Lorentzian (90/10) product function and after subtracting a Shirley background.

Elemental analyses were carried out in a LECO CHNS-932 Analyser. The technique involved sample combustion at 1000°C in an oxygen rich environment. The products of combustion (CO_2, H_2O, and N_2) were carried through the system by He carrier gas. The combustion products were measured quantitatively by means of a non-dispersive IR absorption detection system, except for the N_2 that was determined via a thermal conductivity detector (TC).

Results and Discussion

As mentioned above, the DESs of choice (e.g. DES-ReHy12 and DES-ReHy13) were based on ternary mixtures of Re, Hy and TEA in two different molar ratios (1:2:1 and 1:3:1.75, respectively). DESs were simply obtained by thermally treating (at 90°C) the physical mixture of the components. The melting points of both DES-ReHy12 and DES-ReHy13 (T_m = 64.6 and 47.3°C, respectively, in Fig. 1) were well below those of the individual components (110°C for Re, 129°C for Hy, and 286°C for TEA). The formation of hydrogen bond complexes between Re/Hy and TEA was also confirmed by the upfield chemical shift of the signals ascribed to Re, Hy and TEA in the ^{1}H NMR spectra of the mixtures (see Fig. S1 and Table 1).

Polycondensation of DES-ReHy12 and DES-ReHy13 was confirmed by ^{13}C NMR and FTIR spectroscopies (see Fig. S2 and S3, respectively). According to these spectra (see supporting information for a detailed discussion of peaks assignment), polycondensation proceeded as recently described for similar Hy-based DES prepared with ChCl rather than with TEA.[30] Briefly, Re and Hy – forming part of the DES – were co-condensed by addition of an aqueous solution of formaldehyde and Na_2CO_3. We have previously described how this addition caused partial DES dilution, the occurrence of which was actually beneficial for polycondensation because of the further availability of Re and Hy.[24, 30, 39, 40, 41]

The excellent carbon conversions (e.g. 51–81%, see Table 2) obtained after carbonization – in N_2 atmosphere – of the washed gels confirmed the occurrence of co-condensation between Re and Hy. Actually, conversions at carbonization temperatures between 450 and 700°C (see C_{ReHy12}@450, C_{ReHy12}@500, C_{ReHy12}@600,

C_{ReHy12}@700, C_{ReHy13}@450, C_{ReHy13}@500, C_{ReHy13}@600, and C_{ReHy13}@700 in Table 2) were in the range of those found for self-condensation of Re,[24] and only experienced a significant decrease when the carbonization temperature was 800°C (C_{ReHy12}@800 and C_{ReHy13}@800 also in Table 2). It is worth noting that the use of Hy allowed the formation N-doped carbons, the nitrogen content of which (see Table 1) depended on both the Re/Hy molar ratio used for DES preparation and the carbonization temperature. Thus, as a general rule, low Re/Hy molar ratios rendered N-doped carbons with high nitrogen contents regardless the temperature used for carbonization while, for a given Re/Hy ratio, the nitrogen content tended to decrease if the temperature used for carbonization surpasses 600°C. This latter situation was particularly noticeable when the carbonization temperature approaches 800°C, with the subsequent detrimental effect in terms of carbon conversion (Table 2).[28]

The nature of the nitrogen functionalities was studied by XPS. Up to five types of nitrogen (pyridinic-N at 398.7 ± 0.3 eV, pyrrolic-N or pyridone-N at 400.3 ± 0.3 eV, quaternary-N at 401.4 ± 0.5 eV and oxidized-N at 402–405 eV) can be distinguished in carbonaceous materials by deconvolution analysis of the N_{1s} electron binding energy distribution (Fig. 2 and Table S1).[42, 43] In our case, pyridinic-N, pyrrolic-N or pyridone-N, and quaternary-N (graphitic)[44] were the main nitrogen types found in every sample no matter the thermal treatment. The intensity ratio of pyridinic-N versus quaternary-N groups decreased along with the temperature (within the 450–800°C range) as consequence of the concomitant rearrangement of the carbon network (Fig. 2).[45] XPS also revealed the presence – as a minor component – of oxidized-N in every sample.

The resulting carbon monoliths exhibited a bicontinuous macroporous network, resembling that obtained by means of spinodal decomposition processes (Fig. 3). In our case, Re and Hy co-condensation resulted in the formation of a polymer-rich phase that was accompanied by the segregation of the non-condensed matter – e.g. TEA. The presence of a further pore network – e.g. within the meso or micropore range – was investigated by gas adsorption using different probes (N_2 at 77 K and CO_2 at 273 K). Except for C_{ReHy13}@800, the N_2 uptake at 77 K was negligible in both C_{ReHy12} and C_{ReHy13} samples. This feature could be due to either a poor textural development or the presence of narrow micropores through which the diffusion of the gas at cryogenic temperatures is restricted (Table 2). The latter was confirmed by CO_2 adsorption

isotherms at 273 K using the application of the Dubinin–Radushkevich and Stoeckli–Ballerini equations to calculate the micropore volume (W_0), and the characteristic energy of adsorption (E_0) and average micropore size (L), respectively (Table 2).[46, 47, 48] We observed that, as a general trend, the use of high carbonization temperatures resulted in carbons with smaller micropore diameter and higher micropore volume. Thus, the hierarchical porous structure was composed of macro- and micropores in every case.

The CO_2 adsorption capacity of C_{ReHy12} and C_{ReHy13} at both 273 and 298 K were similar for samples carbonized at the same temperature. For instance, both C_{ReHy12}@800 and C_{ReHy13}@800 reached CO_2 uptakes of ca. 3.7 mmol/g at 273 K and of ca. 2.7 mmol/g at 298 K (Fig. 4, Table 2). Meanwhile, the CO_2 uptake decreased from 3.7 to 1.7 mmol/g at 273 K and from 2.7 to 1.2 mmol/g at 298 K along with the temperature used for carbonization (Table 2). Besides the CO_2 adsorption capacity, we also explored the selectivity of CO_2 versus N_2 adsorption at 298 K. In this case, the carbons carbonized at low temperatures (e.g. 450-500°C, see Table 3) exhibited the best CO_2/N_2 selectivity. CO_2/N_2 selectivity was also evaluated in the Henry law regime that accounts for the low partial pressure region and, hence, can be representative of flue-gas streams characteristic of post-combustion and natural gas fields. Besides the screening of the gas adsorption selectivity at low partial pressures, the Henry's law constant, k_H, can also provide a preliminary assessment of gas–solid interactions because it is related to the gas–adsorbent affinity at infinite dilution.[49] For instance, both C_{ReHy12} and C_{ReHy13} exhibited k_H values for CO_2 that increased along with the temperature used for carbonization in agreement with the CO_2 adsorption capacities described above. With regard to the CO_2/N_2 selectivity, every carbon exhibited k_H values for CO_2, at least, 40-fold higher than their respective k_H values for N_2. The CO_2/N_2 selectivity reached the highest values in carbons obtained at 500°C (see C_{ReHy12}@500 and C_{ReHy13}@500 in their respective series at Table 3). Nonetheless, it is worth mentioning the exceptional value of ca. 96 reached by C_{ReHy13}@700 (see Table 2) most likely due to the favourable combination of very narrow micropores (0.50 nm in diameter) with yet high nitrogen content (7.1 wt %). In any case, the low k_H value found for N_2 in every carbon was indicative of a pronounced size exclusion effect that typically results when the porous morphology resembles that of molecular sieves, that

is, bottleneck-type with wide pore bodies (of around 0.5-0.6 nm in our case, according to Stoeckli–Ballerini equation) and narrow pore entrances that prevented N_2 diffusion into the pore bodies.

We further investigated the selectivity of these carbons by the application of the IAST to predict binary mixture adsorption behaviours from the experimental single component adsorption isotherms of CO_2 and N_2.[50, 51, 52] Data corresponding to the selectivities predicted by the IAST to CO_2–N_2 mixtures representative of synthetic flue gases in post-combustion processes (e.g. with a v/v gas composition of 15/85) and to mixtures with a v/v gas composition of 50/50 is depicted in Table 3. The selectivity calculated by the IAST equation for both binary mixtures (e.g. 15/85 and 50/50) followed a similar trend than those not only obtained from the single component gas data but also calculated from Henry's constants, this is, both C_{ReHy12}@500 and C_{ReHy13}@500 exhibited the highest selectivity (e.g. 41.1 and 63.1, respectively) of their respective series. IAST selectivity was always lower than those obtained from Henry's law, which revealed our carbons as particularly suitable for CO_2–N_2 separation processes carried out at low pressures. Nonetheless, it is worth noting that the CO_2 adsorption capacity of both C_{ReHy12}@500 and C_{ReHy13}@500 was just moderate (e.g. 2.3 and 2.5 mmol/g at 273 K, respectively) as compared to that of samples carbonized at 800 °C (see Table 2).

At this stage, we considered convenient to compare the performance of the HNCMSs herein described with that of other carbons (e.g. HNCs and HCMSs) also prepared using DES-assysted syntheses.[30, 31] Thus, for samples equally carbonized at 800°C, both the CO_2 adsorption capacity and the CO_2/N_2 selectivity exhibited by HNCMSs at 298 K were similar to those found for HCNs and HCMSs – with CO_2 uptakes of up to 3.3 mmol/g and 2.2 mmol/g and the CO_2/N_2 selectivity of up to 8.4 and 6.2, respectively (Table 3). Interestingly, the CO_2/N_2 selectivity of HNCMSs carbonized at 450 and 500°C exhibited a superior performance than any of the carbons obtained from DESs at 800°C, neither those herein reported nor previous ones.

To understand these findings, we need to recall that the size and functionality (e.g. nitrogen moieties) of the pores, and the micropore volume are the main parameters governing both the CO_2-uptake capacity and selectivity.[53] Thus, when adsorption follows a volume filling mechanism, micropores of small diameters (ca.

below 0.8 nm) favoured CO_2 uptake because of the enhanced adsorption potential in the walls of these narrow micropores.[54, 55] In these cases, the larger the micropore volume, the higher the CO_2-uptake capacity. Furthermore, it is widely accepted that the CO_2-uptake capacity enhances with the presence of nitrogen functionalities because the affinity adsorbent-probe is favoured via specific interactions. This is why, besides pore size, nitrogen functionalities play a critical role – more than micropore volume – for the preferential adsorption of CO_2 versus other gases – e.g. CO_2/N_2 selectivity. Thus, N-doping has been largely envisaged to promote the selective adsorption of acidic gases (e.g. CO_2) versus non-acidic ones (e.g. N_2). Moreover, selective adsorptions may be controlled by the size of the pore entrances that discriminates between molecules of different sizes (molecular sieving effects) due to kinetic and/or accessibility restrictions. In this latter case, the narrower is the micropore entrance, the more selective is the adsorption of gases having small kinetic diameters (e.g. 0.33 nm for CO_2) over those having large ones (e.g. 0.36 nm for N_2). According to this discussion, we could conclude that in our samples, where the pore diameter was always below 0.6 nm, the micropore volume prevailed over nitrogen functionalities as the main factor governing the CO_2 adsorption capacity (Fig. 5). Actually, an approximately linear relationship could be observed when the CO_2 adsorption capacity of our carbons was plotted against the micropore volume (Fig. 5). Meanwhile, the nitrogen content seemed to play a more critical role with regard to the CO_2/N_2-selectivity performance. Actually, those carbons with the highest nitrogen contents always exhibited the best performance in terms of CO_2/N_2-selectivity, both at equilibrium, at low pressures and calculated from IAST simulations. In this latter case, Fig. 6 revealed a clear correlation between selectivity and nitrogen content.

These data revealed that the performance of our carbons in terms of both adsorption capacity and CO_2–N_2 selectivity was comparable to – or even better than – those recently reported for the most successful sorbents (Table 3).[56, 57, 58, 59, 60, 61, 62, 63, 64, 65, 66, 67, 68, 69] Particularly interesting was the CO_2–N_2 selectivity at low pressures – and even those calculated by the IAST equation – exhibited by some of our carbons. Thus, the performance calculated from Henry's constants was superior to that described for most recent carbons[31, 32, 70, 71] and only surpassed by certain zeolites.[72, 73, 74, 75] For instance, C_{ReHy13}@700 exhibited a quite remarkable CO_2–N_2 selectivity in the Henry law

regime (ca. 96) while preserving a very decent CO_2-sorption capability (up to 2.8 at 273 K). Meanwhile, in terms of IAST predictions, our carbons were in range to the best carbons recently described[76, 77] and only some organic frameworks have been capable of providing further efficiency.[78, 79, 80]

Conclusions

We have described the preparation of hierarchical porous (bimodal, with micro- and macropores) nitrogen-doped carbons using a DES-assisted synthesis. DESs were composed of resorcinol and 3-hydroxypyridine (as hydrogen donors) and tetraethylammonium bromide (as hydrogen acceptor) so that 3-hydroxypyridine acted as the nitrogen source of the resulting carbons while the presence of tetraethylammonium bromide determined the formation of a molecular sieve structure. In combination with the use of different carbonization temperatures, this DES-assisted synthesis demonstrated a remarkable capability to tailor the hierarchical-type porous structure with macro and micropores and to control the carbon composition with nitrogen contents of up to 8.7 wt %. Besides, the good carbon conversions provided by the precursors forming part of the DES and the full recovery capability of the other DES component provides a reagent economy that emphasizes the low cost character of the synthesis. Considering all these features, the resulting carbons were quite attractive for CO_2 adsorption and CO_2–N_2 separation processes. In terms of performance, we obtained a set of carbons that exhibited CO_2 adsorption capacities of up to 3.7 mmol/g and CO_2–N_2 selectivities of up to 14.4 from single component gas data. It is worth noting that the main factor governing the CO_2 adsorption capacity was the micropore volume while nitrogen content played a more critical role for the preferential adsorption of CO_2 versus other gases. These features, besides the low-cost character of our carbons, open interesting perspectives for their application as sorbents in separation technologies for CO_2 low-pressure post-combustion processes and natural gas upgrading.

Acknowledgments

This work was supported by MINECO (MAT2009-10214, MAT2011-25329, CTM2011-23378, and MAT2012-34811). DC and JP acknowledge MINECO for a JdelaC research contract and a FPI fellowship, respectively.

References

1 N. MacDowell, N. Florin, A. Buchard, J. Hallett, A. Galindo, G. Jackson, C. S. Adjiman, C. K. Williams, N. Shah, and Paul Fennell, "An overview of CO_2 capture technologies" *Energy Environ. Sci.*, **2010**, *3*, 1645–1669

2 S. Choi, J. H. Drese and C. W. Jones, "Adsorbent Materials for Carbon Dioxide Capture from Large Anthropogenic Point Sources" *ChemSusChem*, **2009**, *2*, 796.

3 S. E. Jee and D. S. Sholl, "Carbon Dioxide and Methane Transport in DDR Zeolite: Insights from Molecular Simulations into Carbon Dioxide Separations in Small Pore Zeolites" *J. Am. Chem. Soc.*, **2009**, *131*, 7896.

4 J. C. Hicks, J. H. Drese, D. J. Fauth, M. L. Gray, G. Qi, and C. W. Jones, "Designing Adsorbents for CO_2 Capture from Flue Gas-Hyperbranched Aminosilicas Capable of Capturing CO_2 Reversibly" *J. Am. Chem. Soc.*, **2008**, *130*, 2902-2903.

5 J. Li, Y. Ma, M. C. McCarthy, J. Sculley, J. Yu, H. Jeong, P. B. Balbuena, and H. Zhou, "Carbon dioxide capture-related gas adsorption and separation in metal-organic frameworks" *Coord. Chem. Rev.*, **2011**, *255*, 1791-1823.

6 S. Q. Ma and H. C. Zhou, "Gas storage in porous metal–organic frameworks for clean energy applications" *Chem. Commun.*, **2010**, *46*, 44-53.

7 R. Banerjee, A. Phan, B. Wang, C. Knobler, H. Furukawa, M. O'Keeffe and O. M. Yaghi, "High-Throughput Synthesis of Zeolitic Imidazolate Frameworks and Application to CO_2 Capture" *Science*, **2008**, *319*, 939-943.

8 X. Zhu, P. C. Hillesheim, S. M. Mahurin, C. Wang, C. Tian, S. Brown,H. Luo,G. M. Veith, K. S. Han, E. W. Hagaman, H. Liu, and S. Dai, "Efficient CO_2 Capture by Porous, Nitrogen-Doped Carbonaceous Adsorbents Derived from Task-Specific Ionic Liquids" *ChemSusChem*, **2012**, *5*, 1912–1917.

9 G.-P. Hao, W.-C. Li, D. Qian, and A.-H. Lu, "Rapid Synthesis of Nitrogen-Doped Porous Carbon Monolith for CO_2 Capture" *Adv. Mater.* **2010**, *22*, 853–857

10 A. Wahby, J. M. Ramos-Fernandez, M. Martinez-Escandell, A. Sepulveda-Escribano, J. Silvestre-Albero and F. Rodriguez- Reinoso, "High-Surface-Area Carbon Molecular Sieves for Selective CO_2 Adsorption" *ChemSusChem*, **2010**, *3*, 974.

[11] M.-M. Titirici, R. J. White, C. Falco, and M. Sevilla, "Black perspectives for a green future: hydrothermal carbons for environment protection and energy storage" *Energy Environ. Sci.*, **2012**, *5*, 6796–6822

[12] M. Sevilla, C. Falco, M.-M. Titirici, and A. B. Fuertes "High-performance CO_2 sorbents from algae" *RSC Advances* **2012**, *2*, 12792-12797.

[13] M. Sevilla and A. B. Fuertes, "Sustainable porous carbons with a superior performance for CO_2 capture" *Energy Environ. Sci.*, **2011**, *4*, 1765– 1771.

[14] W. Shen and W. Fan, "Nitrogen-containing porous carbons: synthesis and application" *J. Mater. Chem. A* **2013**, *1*, 999–1013.

[15] For a recent review, see: S. Nardecchia, D. Carriazo, M. C. Gutiérrez, M. L. Ferrer, and F. del Monte, "Three dimensional macroporous architectures and aerogels built of carbon nanotubes and/or graphene: synthesis and applications" *Chem. Soc. Rev.* **2013**, *42*, 794–830.

[16] Y. Huang, H. Cai, D. Feng, D. Gu, Y. Deng, B. Tu, H. Wang, P. A. Webley, and D. Zhao, "One-step hydrothermal synthesis of ordered mesostructured carbonaceous monoliths with hierarchical porosities" *Chem. Commun.* **2008**, 2641.

[17] M. C. Gutiérrez, F. Picó, F. Rubio, J. M. Amarilla, F. J. Palomares, M. L. Ferrer, F. del Monte, and J. M. Rojo, "PPO_{15}-PEO_{22}-PPO_{15} block copolymer assisted synthesis of monolithic macro- and microporous carbon aerogels exhibiting high conductivity and remarkable capacitance." *J. Mater. Chem.* **2009**, *19*, 773–780.

[18] L. Estevez, R. Dua, N. Bhandari, A. Ramanujapuram, P. Wang, and E. P. Giannelis, "A facile approach for the synthesis of monolithic hierarchical porous carbons – high performance materials for amine based CO_2 capture and supercapacitor electrode" *Energy Environ. Sci.*, **2013**, *6*, 1785–1790.

[19] A. P. Abbott, G. Capper, D. L. Davies, R. K. Rasheed and V. Tambyrajah, "Novel solvent properties of choline chloride/urea mixtures" *Chem. Commun.* **2003**, 70–71.

[20] A. P. Abbott, R. C. Harris, and K. S. Ryder, "Application of Hole Theory to Define Ionic Liquids by their Transport Properties" *J. Phys. Chem. B* **2007**, *111,* 4910–4913

[21] A. P. Abbott, G. Capper, and S. Gray, "Design of Improved Deep Eutectic Solvents Using Hole Theory" *ChemPhysChem.* **2006**, *7,* 803–806.

[22] A. P. Abbott, D. Boothby, G. Capper, D. L. Davies, and R. K. Rasheed, "Deep Eutectic Solvents Formed between Choline Chloride and Carboxylic Acids: Versatile Alternatives to Ionic Liquids" *J. Am. Chem. Soc.* **2004**, *126,* 9142–9147.

[23] M. Francisco, A. van den Bruinhorst, and M. C. Kroon, "Low-Transition-Temperature Mixtures (LTTMs): A New Generation of Designer Solvents" *Angew. Chem.* **2013**, *52*, 3074–3085.

[24] D. Carriazo, M. C. Gutiérrez, M. L. Ferrer and F. del Monte, "Resorcinol-Based Deep Eutectic Solvents as Both Carbonaceous Precursors and Templating Agents in the Synthesis of Hierarchical Porous Carbon Monoliths" *Chem. Mater.* **2010**, *22*, 6146–6152.

[25] For a recent review, see: D. Carriazo, M. C. Serrano, M. C. Gutiérrez, M. L. Ferrer, and F. del Monte, "Deep Eutectic Solvents in Polymerizations: A Greener Alternative to Conventional Syntheses" *ChemSusChem* **2013**, DOI: 10.1002/cssc.201300864.

[26] M. C. Gutiérrez, D. Carriazo, A. Tamayo, R. Jiménez, F. Picó, J. M. Rojo, M. L. Ferrer and F. del Monte, "Deep Eutectic Solvents Assisted Synthesis of Hierarchical Carbon Electrodes Exhibiting Capacitance Retention at High Current Densities" *Chem.-A Eur. J.* **2011**, *17*, 10553–10537.

[27] D. Carriazo, M. C. Gutiérrez, F. Picó, J. M. Rojo, J. L. G. Fierro, M. L. Ferrer and F. del Monte, "Phosphate-Functionalized Carbon Monoliths from Deep Eutectic Solvents and their Use as Monolithic Electrodes in Supercapacitors" *ChemSusChem.* **2012**, *5*, 1405–1409.

[28] D. Carriazo, M. C. Gutiérrez, R. Jiménez, M. L. Ferrer and F. del Monte, "Deep-Eutectic-Assisted Synthesis of Bimodal Porous Carbon Monoliths with High Electrical Conductivities" *Part. Part. Sys. Charact.* **2013**, *30*, 316–320.

[29] For a recent review, see: D. Carriazo, M. C. Serrano, M. C. Gutiérrez, M. L. Ferrer, and F. del Monte, "Deep-eutectic solvents playing multiple roles in the synthesis of polymers and related materials" *Chem. Soc. Rev.* **2012**, *41*, 4996–5014.

[30] M. C. Gutiérrez, D. Carriazo, C. O. Ania, J. L. Parra, M. L. Ferrer and F. del Monte, "Deep Eutectic Solvents as Both Precursors and Structure Directing Agents in the Synthesis of Nitrogen Doped Hierarchical Carbons Highly Suitable for CO_2 Capture" *Energy Environ. Sci.* **2011**, *4*, 4201–4210.

[31] J. Patiño, M. C. Gutiérrez, D. Carriazo, C. O. Ania, J. L. Parra, M. L. Ferrer and F. del Monte, "Deep eutectic assisted synthesis of carbon adsorbents highly suitable for low-pressure separation of CO_2–CH_4 gas mixtures" *Energy Environ. Sci.* **2012**, *5*, 8699–8707.

[32] X. Ma, M. Cao, and C. Hu, "Bifunctional HNO_3 catalytic synthesis of N-doped porous carbons for CO_2 capture" *J. Mater. Chem. A*, **2013**, *1*, 913

[33] F. Su, C. K. Poh, J. S. Chen, G. Xu, D. Wang, Q. Li, J. Lin, and X. W. Lou, "Nitrogen-containing microporous carbon nanospheres with improved capacitive properties" *Energy Environ. Sci.*, **2011**, *4*, 717-724

[34] S. Li, J. L. Falconer, and R. D. Noble, "Improved SAPO-34 Membranes for CO_2/CH_4 Separations" *Adv. Mater.* **2006**, *18*, 2601–2603

[35] M. A. Carreon, S. Li, J. L. Falconer, and R. D. Noble, "SAPO-34 Seeds and Membranes Prepared Using Multiple Structure Directing Agents" *Adv. Mater.* **2008**, *20*, 729–732

[36] L. Czepirski and J. Jagiełło, "Virial-type thermal equation of gas–solid adsorption" *Chem. Eng. Sci.*, **1989**, *44*, 797–801.

[37] A. L. Myers and J. M. Prausnitz, "Prediction of the adsorption isotherm by the principle of corresponding slates" *AIChE J.*, **1965**, *11*, 121–127.

[38] C. R. C. Jensen and N. A. Seaton, "An Isotherm Equation for Adsorption to High Pressures in Microporous Adsorbents" *Langmuir*, **1996**, *12*, 2866–2867.

[39] M. C. Gutiérrez, C. R. Mateo, M. L. Ferrer, and F. del Monte, "Freeze-Drying of Aqueous Solutions of Deep Eutectic Solvents: A Suitable Approach to Deep Eutectic Suspensions of Self-Assembled Structures" *Langmuir* **2009**, *25*, 5509– 5515.

[40] M. C. Gutiérrez, M. L. Ferrer, L. Yuste, F. Rojo, and F. del Monte, "Bacteria Incorporation in Deep Eutectic Solvents via Freeze-Drying." *Angew. Chem.* **2010**, *49*, 2158–2162

[41] S. Nardecchia, M. C. Gutiérrez, M. L. Ferrer, M. Alonso, I. Lopez, J. C. Rodriguez-Cabello, and F. del Monte, "Phase Behaviour of Elastin-Like Synthetic Recombinamers in Deep Eutectic Solvents" *Biomacromolecules* **2012**, *13*, 2029–2036.

[42] F. Kapteijn, J. A. Moulijn, S. Matzner and H.-P. Boechm, "The development of nitrogen functionality in model chars during gasification in CO_2 and O_2" *Carbon*, **1999**, *37*, 1143–1150.

[43] J. R. Pels, F. Kapteijn, J. A. Moulijn, Q. Zhu and K. M. Thomas, "Evolution of nitrogen functionalities in carbonaceous materials during pyrolysis" *Carbon*, **1995**, *33*, 1641–1653.

[44] M. Pérez-Cadenas, C. Moreno-Castilla, F. Carrasco-Marín and A. F. Pérez-Cadenas, "Surface Chemistry, Porous Texture, and Morphology of N-Doped Carbon Xerogels" *Langmuir*, **2009**, *25*, 466–470.

[45] M. Seredych, D. Hulicova-Jurcakova, G. Q. Lu and T. J. Bandosz, "Surface functional groups of carbons and the effects of their chemical character, density and accessibility to ions on electrochemical performance" *Carbon*, **2008**, *46*, 1475–1488.

[46] J. Garrido, A. Linares-Solano, J. M. Martın-Martınez, M. Molina-Sabio, F. Rodrıguez-Reinoso, and R. Torregrosa, "Use of nitrogen vs. carbon dioxide in the characterization of activated carbons" *Langmuir*, **1987**, *3*, 76–81.

[47] C. O. Ania, J. B. Parra, F. Rubiera, A. Arenillas and J. J. Pis, "A comparison of characterization methods based on N_2 and CO_2 adsorption for the assessment of the pore size distribution of carbons" *Stud. Surf. Sci. Catal*., **2007**, *160***,** 319–326.

[48] J. Silvestre-Albero, A. Silvestre-Albero, F. Rodríguez-Reinoso and M. Thommes, "Physical characterization of activated carbons with narrow microporosity by nitrogen (77.4 K), carbon dioxide (273 K) and argon (87.3 K) adsorption in combination with immersion calorimetry" *Carbon*, **2011**, *50*, 3128–3133

[49] J. Jagiełło, T. J. Bandosz, K. Putyera and J.A. Schwarz, "Adsorption near Ambient Temperatures of Methane, Carbon Tetrafluoride, and Sulfur Hexafluoride on Commercial Activated Carbons" *Chem. Eng. Data*, **1995**, *40*, 1288–1292

[50] S. Himeno, T. Tomita, K. Suzuki and S. Yoshida, "Characterization and selectivity for methane and carbon dioxide adsorption on the all-silica DD3R zeolite" *Micropor. Mesopor. Mater.*, **2007**, *98*, 62–67.

[51] V. Goetz, O. Pupier and A. Guillot, "Carbon dioxide-methane mixture adsorption on activated carbon" *Adsorption,* **2006**, *12*, 55–63.

[52] B. Liu and B. Smit, "Molecular Simulation Studies of Separation of CO_2/N_2, CO_2/CH_4, and CH_4/N_2 by ZIFs" *J. Phys. Chem. C*, **2010**, *114*, 8515–8522.

[53] M. Sevilla, J. B. Parra, and A. B. Fuertes, "Assessment of the Role of Micropore Size and N-Doping in CO_2 Capture by Porous Carbons" *ACS Appl. Mater. Interfaces*, **2013**, *5*, 6360–6368

[54] S. J. Gregg, K. S. W. Sing, in "Adsorption, surface area and porosity." Academic Press, 1991

[55] F. Rouquerol, J. Rouquerol, K. Sing, in "Adsorption by powders and porous solids: principles, methodology and applications." Academic Press, 1999

[56] M. Sevilla and A. B. Fuertes, "Sustainable porous carbons with a superior performance for CO_2 capture" *Energy Environ. Sci.*, **2011**, *4*, 1765–1771

[57] M. Sevilla, P. Valle-Vigón and A. B. Fuertes, "N-Doped Polypyrrole-Based Porous Carbons for CO_2 Capture" *Adv. Funct. Mater.*, **2011**, *21*, 2781–2787

[58] L. Wang and R. T. Yang, "Significantly Increased CO_2 Adsorption Performance of Nanostructured Templated Carbon by Tuning Surface Area and Nitrogen Doping" *J. Phys. Chem. C*, 2012, **116**, 1099–1106

[59] Z. Zhang, J. Zhou, W. Xing, Q. Xue, Z. Yan, S. Zhuo, and S. Z. Qiao, "Critical role of small micropores in high CO2 uptake" *Phys. Chem. Chem. Phys.*, **2013**, *15*, 2523−2529

[60] X. Fan, L. Zhang, G. Zhang, Z. Shu, and J. Shi, "Chitosan derived nitrogen-doped microporous carbons for high performance CO_2 capture" *Carbon* **2013**, *61*, 423−430

[61] L. Liu, J. Yang, J. Li, J. Dong, D. Šišak, M. Luzzatto and L. B. McCusker, "Ionothermal Synthesis and Structure Analysis of an Open-Framework Zirconium Phosphate with a High CO_2/CH_4 Adsorption Ratio" *Angew. Chem. Int. Ed.*, **2011**, *50*, 8139–8142

[62] S. Cavenati, C. A. Grande, and A. E. Rodrigues, "Adsorption Equilibrium of Methane, Carbon Dioxide, and Nitrogen on Zeolite 13X at High Pressures" *J. Chem. Eng. Data*, **2004**, *49*, 1095−1101

[63] R. Banerjee, H. Furukawa, D. Britt, C. Knobler, M. O'Keeffe and O. Yaghi, "Control of Pore Size and Functionality in Isoreticular Zeolitic Imidazolate Frameworks and their Carbon Dioxide Selective Capture Properties" *J. Am. Chem. Soc.*, **2009**, *131*, 3875–3877

[64] R. Dawson, E. Stöckel, J. R. Holst, D. J. Adams and A. I. Cooper, "Microporous organic polymers for carbon dioxide capture" *Energy Environ. Sci.*, **2011**, *4*, 4239–4245

[65] Y. Jin, B. A. Voss, A. Jin, H. Long, R. D. Noble, and W. Zhang, "Highly CO_2-Selective Organic Molecular Cages: What Determines the CO_2 Selectivity" *J. Am. Chem. Soc.*, **2011**, *133*, 6650–6658

[66] M. G. Rabbani and H. M. El-Kaderi, "Synthesis and Characterization of Porous Benzimidazole-Linked Polymers and Their Performance in Small Gas Storage and Selective Uptake" *Chem. Mater.* **2012**, *24*, 1511−1517

[67] M. G. Rabbani, T. E. Reich, R. M. Kassab, K. T. Jackson, and H. M. El-Kaderi, "High CO_2 uptake and selectivity by triptycene-derived benzimidazole-linked polymers" *Chem. Commun.* **2012**, *48*, 1141−1143

[68] J. An, S. J. Geib, and N. L. Rosi, "High and Selective CO_2 Uptake in a Cobalt Adeninate Metal-Organic Framework Exhibiting Pyrimidine- and Amino-Decorated Pores" *J. Am. Chem. Soc.*, **2010**, *132*, 38–39

[69] Z. Zhang, S. Xian, H. Xi, H. Wang and Z. Li, "Improvement of CO_2 adsorption on ZIF-8 crystals modified by enhancing basicity of surface" *Chem. Eng. Sci.,* 2011, **66**, 4878–4888

[70] G. P Hao, W. C Li, D. Qian, G. H Wang, W. P. Zhang, T. Hang, A. Q. Wang, F. Schüth, H. J. Bongard and A. H. Lu, "Structurally Designed Synthesis of Mechanically Stable Poly(benzoxazine-co-resol)-Based Porous Carbon Monoliths and Their Application as High-Performance CO_2 Capture Sorbents" *J. Am. Chem. Soc.*, **2011**, *133*, 11378–11388.

[71] Y. Jin, S. C. Hawkins, C. P. Huynh, and S. Su, "Carbon nanotube modified carbon composite

monoliths as superior adsorbents for carbon dioxide capture" *Energy Environ. Sci.*, **2013**, *6*, 2591-2596

[72] S. Sircar, T. C. Golden and M. B. Rao, "Activated carbon for gas separation and storage" *Carbon*, **1996**, *34*, 1–12

[73] D. Saha, Z. B. Bao, F. Jia, and S. G. Deng, "Adsorption of CO_2, CH_4, N_2O, and N_2 on MOF-5, MOF-177, and Zeolite 5A" *Environ. Sci. Technol.* **2010**, *44*, 1820−1826

[74] H. Chen, H. Yu, Y. Tang, M. Pan, G. Yang, F. Peng, H. Wang and J. Yang, "Adsorption separation of carbon dioxide, methane, and nitrogen on Hβ and Na-exchanged β-zeolite" *J. Natural Gas Chem.,* **2008**, *17*, 391−396

[75] B. Wang, H. Furukawa, M. O'Keeffe and O. M. Yaghi, "Colossal cages in zeolitic imidazolate frameworks as selective carbon dioxide reservoirs" *Nature*, **2008**, *453*, 207–212

[76] Y. Zhao, L. Zhao, K. X. Yao, Y. Yang, Q. Zhang, and Y. Han, "Novel porous carbon materials with ultrahigh nitrogen contents for selective CO_2 capture" *J. Mater. Chem.* **2012**, *22*, 19726−19731

[77] Y. Zhao, X. Liu, K. X. Yao, L. Zhao, and Y. Han, "Superior Capture of CO_2 Achieved by Introducing Extra-framework Cations into N-doped Microporous Carbon" *Chem. Mater.* **2012**, *24*, 4725−4734

[78] T. Ben, Y. Li, L. Zhu, D. Zhang, D. Cao, Z. Xiang, X. Yao, and S. Qiu, "Selective adsorption of carbon dioxide by carbonized porous aromatic framework (PAF)" *Energy Environ. Sci.* **2012**, *5*, 8370

[79] W. Lu, D. Yuan, J. Sculley, D. Zhao, R. Krishna, and H. C. Zhou, "Sulfonate-Grafted Porous Polymer Networks for Preferential CO_2 Adsorption at Low Pressure" *J. Am. Chem. Soc.*, **2011**, *133*, 18126–18129

[80] Y. Zhu, H. Long, and W. Zhang, "Imine-Linked Porous Polymer Frameworks with High Small Gas (H_2, CO_2, CH_4, C_2H_2) Uptake and CO_2/N_2 Selectivity" *Chem. Mater.* **2013**, *25*, 1630−1635

Table 1: ^{1}H-NMR spectroscopy data of the DESs prepared in this work. The chemical shifts of the DES components themselves – resorcinol (Re), 3-hydroxypyridine (Hy) and tetraetylammonium bromide (TEA) – are included for comparison.

Sample	δ (ppm)									
	HDO	Resorcinol (Re)			3-Hydroxypyridine (Hy)				Tetraethylammonium bromide (T)	
		H at C5	H at C4 & 6	H at C2	H at C6	H at C5	H at C4	H at C2	H at C2	H at C1
Re	4.85[a]	6.99[a]	6.34[a]	6.31[a]						
Hy					7.29[b]	7.33[b]	8.09[b]	8.28[b]		
T	4.76[a]								1.19[a]	3.19[a]
DES-ReHy12		6.16	5.69	5.88	6.40	6.56	7.19	7.53	0.20	2.16
DES-ReHy13		6.19	5.70	5.91	6.45	6.60	7.23	7.60	0.27	2.28

[a] In D_2O [b] In $CDCl_3$

Table 2: Physical-chemistry properties of C_{ReHy12} and C_{ReHy13} samples including nitrogen content, carbon conversion, surface area (obtained from N_2 isotherms at 77 K), textural properties (obtained from CO_2 isotherms at 273 K), and maximum uptake and Henry's constants for N_2 and CO_2.

Sample	Nitrogen Content (wt %)	Conversion (%)	S_{BET} (m^2/g)	L (nm)	E_0 (kJ/mol)	W_0 (cm^3/g)	CO_2 uptake at 273 K – 298 K (mmol/g)	N_2 uptake at 298 K (mmol/g)	Henry's constants	
									k_H for CO_2	k_H for N_2
C_{ReHy12}@450	7.6	80.6	7	0.60	29.4	0.131	1.7 – 1.2	0.1	4.85	0.11
C_{ReHy12}@500	7.7	74.0	22	0.57	30.3	0.169	2.3 – 1.6	0.1	7.90	0.15
C_{ReHy12}@600	7.7	66.5	5	0.56	30.7	0.222	2.9 – 2.1	0.2	12.59	0.26
C_{ReHy12}@700	6.6	66.3	7	0.53	31.6	0.245	3.1 – 2.2	0.4	18.84	0.44
C_{ReHy12}@800	3.7	53.8	4	0.53	31.7	0.270	3.7 – 2.7	0.4	21.44	0.49
C_{ReHy13}@450	8.7	81.4	5	0.56	30.6	0.142	2.0 – 1.4	0.1	7.04	0.17
C_{ReHy13}@500	8.7	76.1	4	0.57	30.4	0.196	2.5 – 1.8	0.1	10.21	0.12
C_{ReHy13}@600	8.1	72.7	2	0.56	30.7	0.242	2.9 – 2.3	0.3	16.63	0.33
C_{ReHy13}@700	7.1	67.9	7	0.50	33.0	0.257	2.8 – 2.4	0.4	24.87	0.26
C_{ReHy13}@800	5.4	51.3	349	0.52	32.2	0.261	3.6 – 2.7	0.5	24.31	0.62

Table 3: CO_2/N_2 selectivity of C_{ReHy12} and C_{ReHy13} obtained at 298 K under equilibrium conditions and from Henry constants at ambient (e.g. 1.2 bars) and low pressures, respectively, and calculated from IAST simulations for different gas mixtures. Data collected from different works are included for comparison. Experimental conditions were similar for every sample unless otherwise specified (see foot note).

Type of sample	Ref.	Equilibrium	Henry	IAST	
		CO_2/N_2	CO_2/N_2	CO_2/N_2 (15:85)	CO_2/N_2 (50:50)
C_{ReHy12}@450	This work	12.9	45.1	6.7	33.1
C_{ReHy12}@500	This work	11.0	52.0	9.5	41.1
C_{ReHy12}@600	This work	8.7	48.6	7.1	30.2
C_{ReHy12}@700	This work	6.4	42.5	5.3	25.7
C_{ReHy12}@800	This work	6.3	43.5	5.4	21.6
C_{ReHy13}@450	This work	10.8	41.2	9.4	38.2
C_{ReHy13}@500	This work	14.4	84.9	13.0	63.1
C_{ReHy13}@600	This work	7.5	50.3	7.5	30.3
C_{ReHy13}@700	This work	6.7	95.9	7.1	28.1
C_{ReHy13}@800	This work	5.5	39.3	4.9	19.3
Carbon Narrow Micropores	30	6.2	30		
Carbon N-doped	31	8.4			
Carbon N-doped	9	10			

Carbon N-doped	56	5.4[a]			
Carbon N-doped	57	5.3[a]			
Carbon N-doped	58	14			
Carbon Narrow Micropores N-doped	59	8[a]			
Carbon N-doped Chitosan derived	60	21[a]			
MOF[f]**:** Zirconium Phosphate	61	4.9[a]			
13X-**Zeolite**	62	20[a, b]			
ZIF[g]-68 **ZIF**-69 **ZIF**-70 **ZIF**-78 **ZIF**-79 **ZIF**-81 **ZIF**-82	63	18 20 17 50 23 24 35			
MOP[h]	64	9-20[a]			
Covalent organic polymers	65	138[c]			
Benzimidazole-linked polymers (MOP)	66		113[d]		
Benzimidazole-linked polymers (MOP)	67		39 63[d]		
MOF	68	31 14[d]	75 81[d]		

O-**ZIF**-8 N-**ZIF**-8 H-**ZIF**-8 A-**ZIF**-8	69		8.42 11.27 12.26 13.15		9.64 13.28 11.90 14.38
Carbon N-doped	32	3.9[a]	30		
Carbon HCM-DAH-1 **Carbon** HCM-DAH-1-900-1 **Carbon** HCM-DAH-1-900-3	70		28 17 13		
Carbon CNT composite monoliths	71		19.8 32.6[d]		
Carbon BPL **Zeolite** 5	72		11.1[a] 330[a]		
MOF-5 MOF-177 Zeolite 5A	73		17.5 17.7 240.6		
H-**β-Zeolite** Na-**β-Zeolite**	74		50.3[a] 25.6[a]		
ZIF-100 **ZIF**-95	75		25 18		
Carbon N-doped IBN9-NC1 **Carbon** N-doped IBN9-NC1-A	76			34[a] 21[a]	
Carbon N-doped KNC-A-K **Carbon** N-doped SBA-NC	77				40[a] 27[a]
Carbonized (at 450 °C) Open Framework	78				209[a, d]

Porous Polymer Network (PPN)	79	45[a, e]	17[e]	414[a, e]	
Covalent organic polymers	80			15[a, d]	

[a] Measured at 1 bar. [b] Measured at 278K. [c] Measured at 293K. [d] Measured at 273K. [e] Measured at 295K. [f] MOF stands for metal organic frameworks. [g] ZIF stands for zeolitic imidazole frameworks. [h] MOP stands for microporous organic poymers.

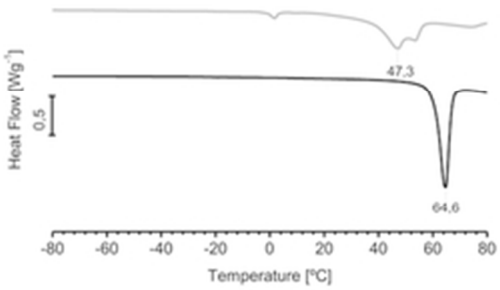

26x14mm (300 x 300 DPI)

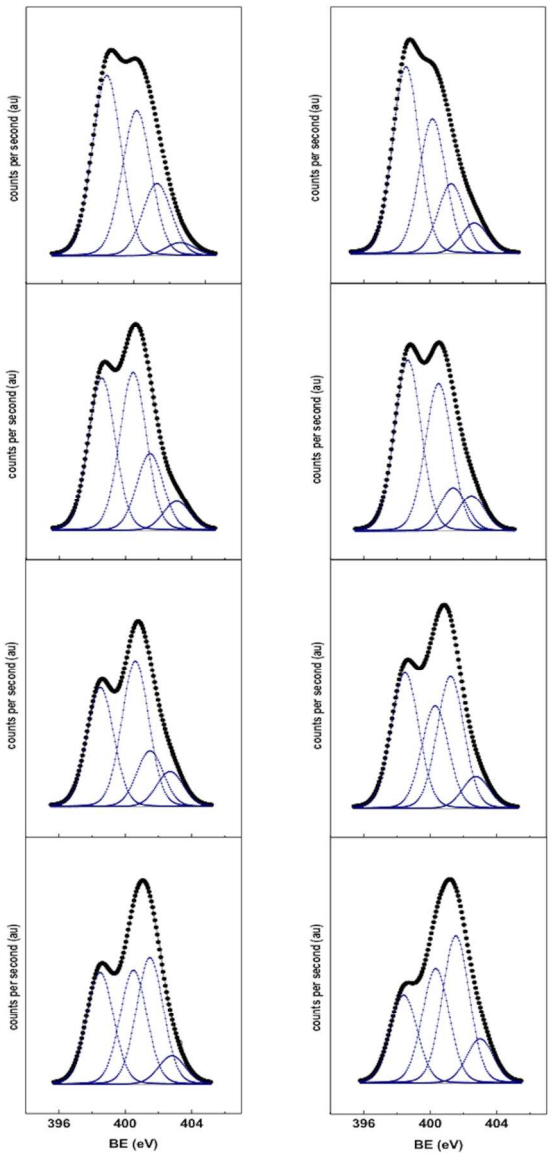

161x324mm (300 x 300 DPI)

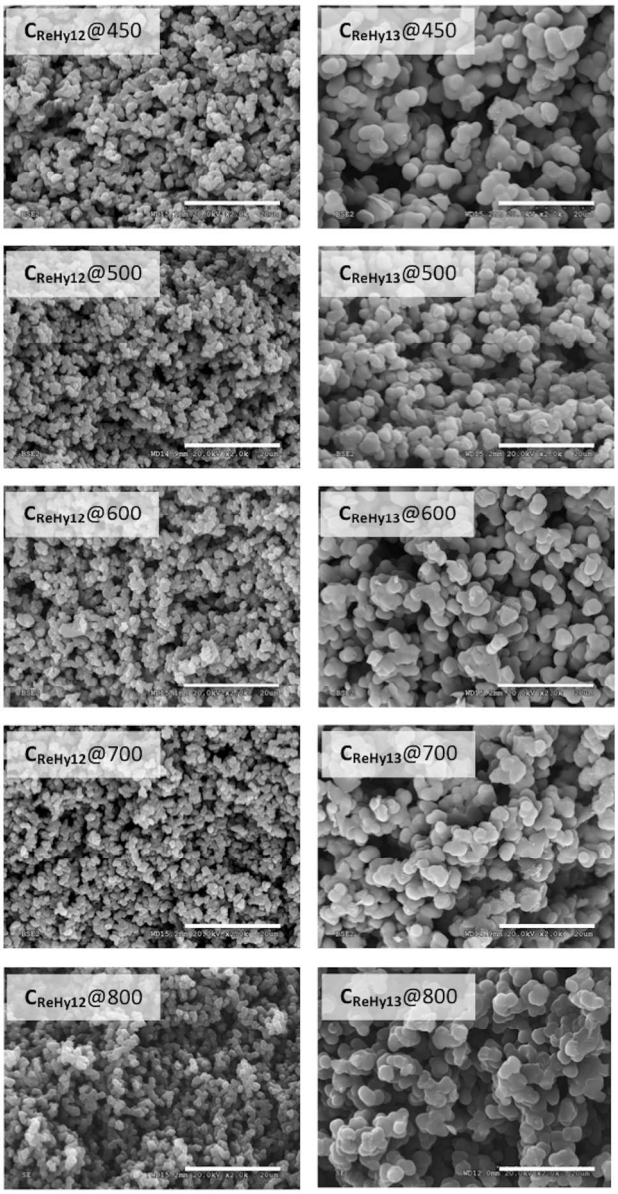

153x294mm (300 x 300 DPI)

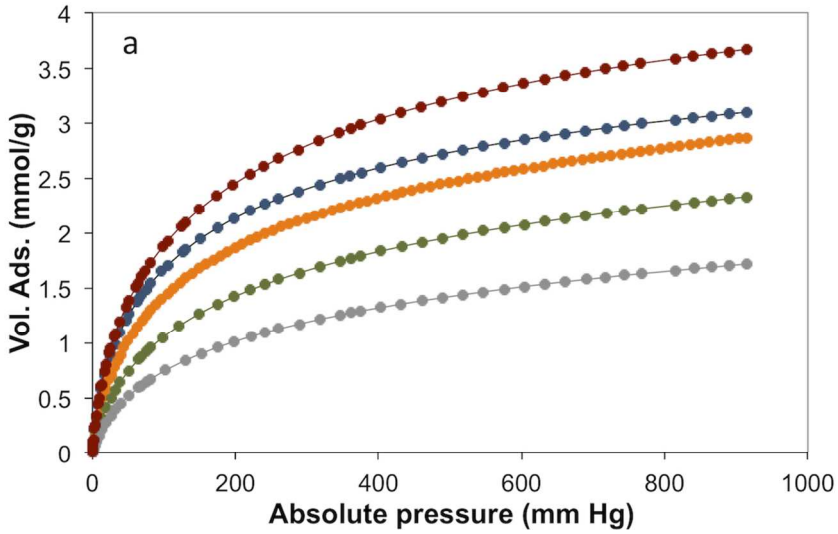

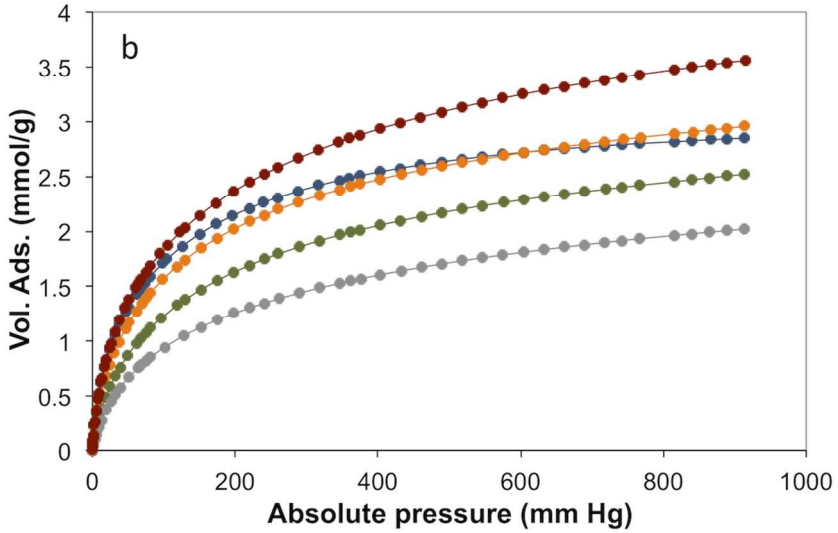

108x147mm (300 x 300 DPI)

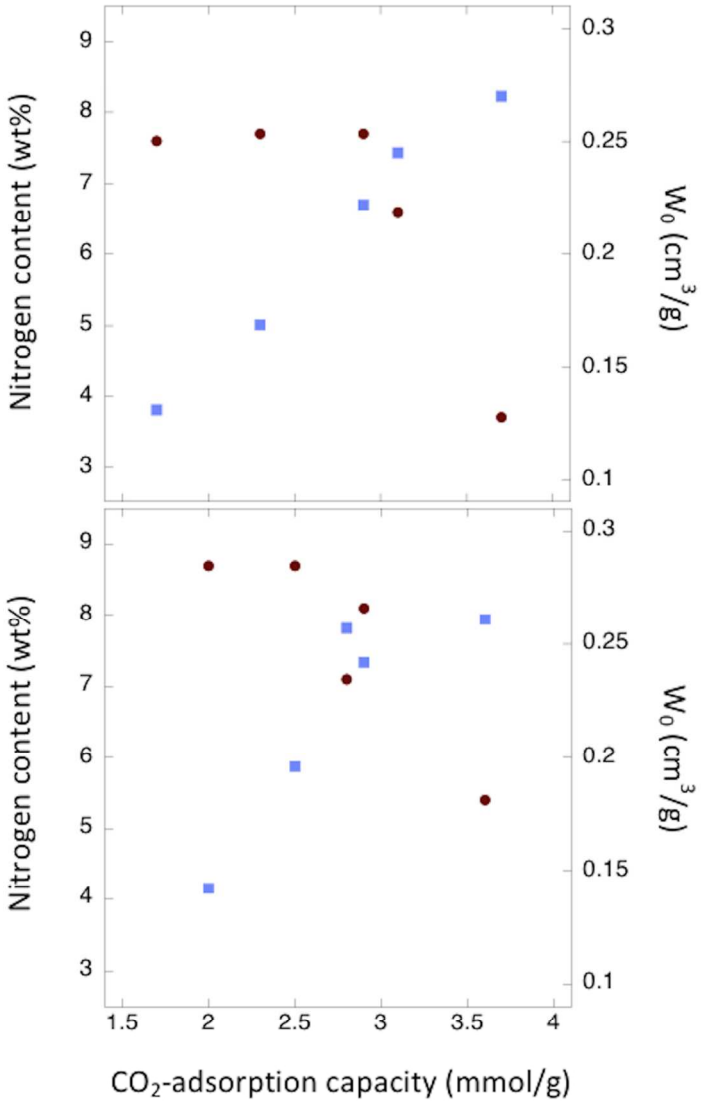

91x140mm (300 x 300 DPI)

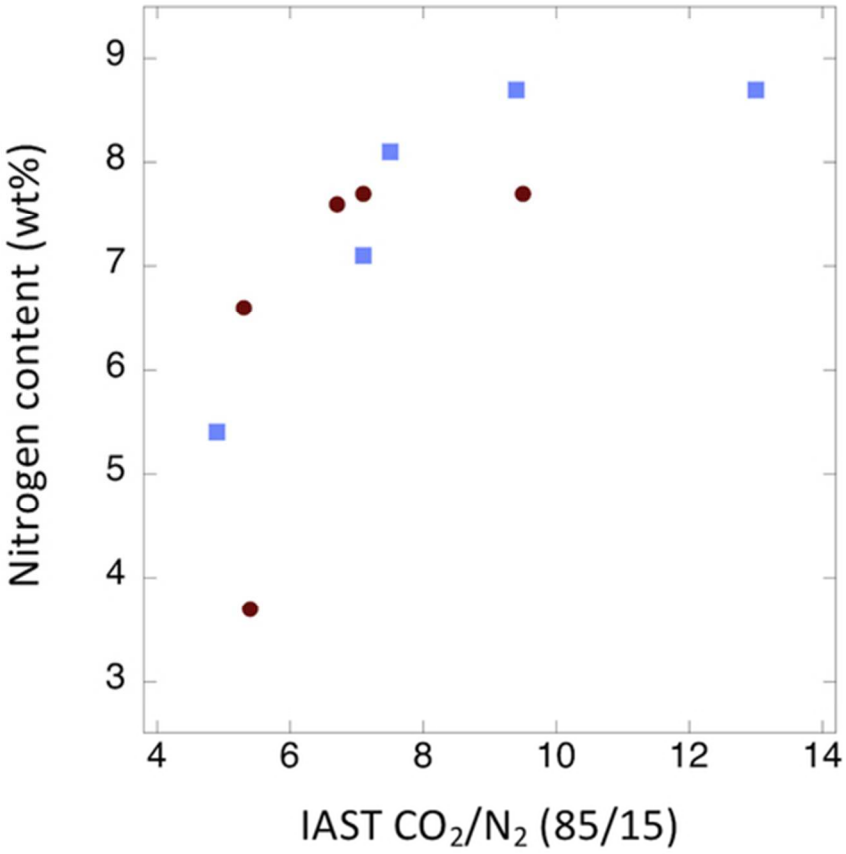

48x47mm (300 x 300 DPI)

Figure 1: DSC traces taken at a rate of 1°C/min of DES-ReHy12 (black line) and DES-ReHy13 (grey line).

Figure 2: XPS N_{1s} of (left column, from top to bottom) C_{ReHy12}@500, C_{ReHy12}@600, C_{ReHy12}@700, and C_{ReHy12}@800, and (right column, from top to bottom) C_{ReHy13}@500, C_{ReHy13}@600, C_{ReHy13}@700, and C_{ReHy13}@800.

Figure 3: SEM micrographs of C_{ReHy12} and C_{ReHy13} showing a homogeneous bicontinuous structure for every temperature used for carbonization. Bar are 20 μm.

Figure 4: CO_2 adsorption isotherms at 273 K of (a) C_{ReHy12}@450 (grey), C_{ReHy12}@500 (green), C_{ReHy12}@600 (orange), C_{ReHy12}@700 (blue), and C_{ReHy12}@800 (red), and (b) C_{ReHy13}@450 (grey), C_{ReHy13}@500 (green), C_{ReHy13}@600 (orange), C_{ReHy13}@700 (blue), and C_{ReHy13}@800 (red).

Figure 5: Plot representing the CO_2 adsorption capacity versus the nitrogen content (left y axis, red symbols) and the micropore volume (right y axis, blue symbols) of C_{ReHy12} (top panel) and C_{ReHy13} (bottom panel) samples.